Arch. Metall. Mater. **69** (2024), 1, 365-373

DOI: https://doi.org/10.24425/amm.2024.149103

K. ŚCIBISZ[1,2*], J. KRAWCZYK[3]

QUANTITATIVE AND QUALITATIVE EVALUATION OF NON-METALLIC INCLUSIONS IN HIGH-SILICON STEEL AFTER HOT ROLLING

This paper presents an analysis of non-metallic inclusions occurring in high-silicon steels containing about 3% Si of terms of their type, volume fraction and morphology. The inclusions were divided into 3 main groups: oxides, sulfides, nitrides which together can also form complex. The work was based on numerous metallographic observations in two sections (longitudinal and transverse to the rolling direction). The study was performed on three casts differing in chemical composition. The analyzed casts were characterized by a different content of non-metallic inclusions, which can be associated with slight differences in chemical composition. The analyzed results showed that the most common inclusions were oxides and nitrides. Sulfides occurred sporadically.

Keywords: Non-metallic inclusions; oxides; sulfides; nitrides; high-silicon steel

1. Introduction

Non-metallic inclusions (NMIs) occur in steels mostly in the form of oxides, sulfides and nitrides and their presence is inevitable in melt steel. They are formed during the steelmaking process, mostly in the liquid steel deoxidation phase, at which stage their amount can be modified by the addition of calcium and the formation of: calcium aluminates of various compositions, calcium sulfide (CaS), manganese sulfide (MnS) and also Al_2O_3-CaO-MgO oxides in various configurations. Hard and solid (at steelmaking temperatures) dispersed oxide inclusions and spinel ($MgAl_2O_4$) transform into liquid calcium aluminate inclusions by applied calcium treatment. The lower density of NMIs relative to the density of the steel causes them to float towards the steel-slag interface due to buoyancy, the steelmaking slags readily dissolve the most common inclusions, this way the most of NMIs can be captured by the slag and removed from the steel but unfortunately not all of them. Further formation of inclusions occurs in the process of continuous casting (CC) of the steel during solidification and temperature reduction. The cooling rate in the CC process influences both the number and size of inclusions, the solute in the steel is rejected from the solidification front and the solute-enriched liquid steel solidifies at the central part of the strand. The uneven solute distribution at the strand centre is usually called central segregation and has a detrimental effect on the final steel product properties [1-6]. It is well known that non-metallic inclusions are harmful to properties of every kind of steel produced worldwide. They can influence various mechanical and physical properties of steel including plastic characteristic, fatigue strength, corrosion resistance. Local corrosion is a consequence of the effect of the electrolyte solution on the inclusion and/or the metal matrix around the inclusion. Their role in the initiation of cracking and fatigue are also studied in research papers [7-10]. In high-silicon steels with a content of approximately 3% Si for the manufacture of conventional grain-oriented (CGO) electrical steels, the effect of NMIs on magnetic properties must be additionally considered. Generally, it can be said that in order to obtain the desired magnetic properties of the material, i.e. low loss and good magnetic permeability, the amount of NMIs should be as low as possible. The presence of precipitates in the size range 10-400 nm can affect directly on the movement of magnetic domains and indirectly by blocking grain growth inhibitions. Inclusions having a size close to the wall thickness of the magnetic domains (100-200 nm) have the greatest impact on coercivity and hysteresis losses, they have the greatest ability to pin to the walls of the magnetic domains [11-13]. In the production of electrical steels, precipitates such as AlN, MnS or CuS play a special role and

[1] ARCELORMITTAL POLAND S.A. UNIT IN KRAKOW, TADEUSZA SENDZIMIRA 1 STR., 31-752 KRAKOW, POLAND
[2] AGH UNIVERSITY OF KRAKOW, FACULTY OF METALS ENGINEERING AND COMPUTER SCIENCE, AGH DOCTORAL SCHOOL, AL. MICKIEWICZA 30, 30-059 KRAKOW, POLAND
[3] AGH UNIVERSITY OF KRAKOW, FACULTY OF METALS ENGINEERING AND COMPUTER SCIENCE, AL. MICKIEWICZA 30, 30-059 KRAKOW, POLAND

* Corresponding author: scibisz@agh.edu.pl

are used as grain growth inhibitors [14]. The strong affinity of aluminum for oxygen and nitrogen in the Fe-Al-O and Fe-Al-N system in the steel favors the formation of high-melting Al_2O_3 and AlN inclusions. The precipitation of AlN usually occurs during the solidification process of the steel, nevertheless, if the proportion of Al is sufficient, it can also occur in liquid steel. The formation process of Al_2O_3 and AlN is strictly dependent on the chemical composition and the percentage of individual elements [15]. In high-silicon steels dedicated to manufacture electrical steel, the proportion of Al and N is strictly controlled due to the need for sufficient AlN content. In order to obtain the desired texture, the so-called Goss texture, and the corresponding material properties, thermomechanical processing and annealing are necessary. The cold rolled sheet is decarburized in the initial annealing process at approx. 850°C, AlN acts to pin the grain boundaries and in the secondary recrystallisation process during annealing at 1100°-1200°C, it is dissolved which promotes grain growth with the desired Goss orientation [16]. Despite years of research, the mechanisms favoring the growth of grains with Goss orientation, are still not well understood. There are several theories that describe the formation process of oriented grains. One of these is the theory pointing to the key role of AlN and MnS as inhibitors. AlN is called an acquired inhibitor because it is not present during the hot and cold rolling process, it forms after the hot rolling process during cooling and in the subsequent recrystallisation annealing stages. Fine and dispersed MnS particles form during hot rolling. Compared to MnS, AlN is a more stable inhibitor in the high temperature range due to its higher melting point, leading to a slower decomposition rate. Depending on the type of inhibitor, a suitable technological process is selected to ensure that the optimum properties of the final product are achieved [17-19].

CGO electrical steels have been the most cost-effective material for use in energy systems for years. Reducing the lossiness of the steel is a major issue in commercial steel production, and manufacturing processes are still being developed to achieve higher quality [20]. However, the potential for further improvements in magnetic properties still depends on careful control of inclusions content during steel production, therefore the aim of this study was to analyze the non-metallic inclusions present in high-silicon steel in terms of their type, quantity and morphology.

2. Material and methods of examination

The investigation of 3 selected heats of high-silicon steel with Si 3.1% content and differing in the content of key elements (TABLE 1) involved in inclusions formation such as Al, N, S, O, Ti were performed. The content of other elements such as Mn or Ca was at the same level for all 3 heats (approximate values Mn 0.28%, Ca 0.0002%).

Analysis of the inclusions was carried out on the polished metallographic specimens prepared from the hot rolled sheets sample cut both longitudinally and transverse to the rolling direction. The samples were prepared on a grinder and polisher

TABLE 1

Key chemical elements composition of examined heats

in % wt. / No. of heat	Al	N	S	O	Ti
1	0.014	0.0056	0.0044	0.0023	0.0006
2	0.013	0.0083	0.0045	0.0013	0.0008
3	0.016	0.0077	0.0050	0.0026	0.0004

machine using a polishing slurry and automatic holders, then rinsed with alcohol and dried. In order to confirm the chemical composition of the individual inclusions, EDS analysis was performed using an Phenom XL SEM microscope. Metallographic observations for quantitative analysis were made using the Carl Zeiss Axiovert 200 MAT optical microscope equipped in camera AxioCam MRc5. During the observations, the shape and color of the inclusions are important to distinguish the type of inclusions, e.g. sulfides from oxides or nitrides. The volume fraction of non-metallic inclusions was determined on non-etched specimens. A "point" method using a grid was used. Measurements of the number of inclusions were made for each sample in both longitudinal and transverse sections. The measurement was based on counting the number of grid nodes lying on the inclusions, distinguishing between the different types of inclusions (nitrides, sulfides, oxides, exogenous inclusions). For each sample, 100 random grid projections were made, i.e. 50 projections per section. The imposed grid covered an area of 1 mm^2 of the given cross-sectional area. The number of grid nodes in each projection was 494 (38 horizontal lines × 13 vertical lines). Testing was performed using a 150× objective magnification.

The volume fraction (Vv) of non-metallic inclusions was calculated using followed formula:

$$V_v = \frac{\sum_{i=1}^{k} P_i}{k \cdot z} \cdot 100\% \qquad [21]$$

Which means:

- k – grid application quantity (50),
- z – the number of grid nodes (494),
- Pi – the number of grid nodes exposed to non-metallic inclusions.

Total content of individual non-metallic inclusions was determined:

$$\text{Total } Vv(i) = \frac{Vv \text{ longitudinal section} + Vv \text{ cross section}}{2}$$

Which means:

- Vv – Volume fraction
- (i) – individual type of non metallic inclusion (oxides, sulfides, nitrides)

Total content of all non-metallic inclusions was determined:

$$\text{Total } Vv = \frac{\text{Total } Vv \text{ sulfides} + \text{Total } Vv \text{ oxides} + \\ + \text{Total } Vv \text{ nitrides}}{3}$$

Non-metallic inclusions were identified on the basis of their morphology, divided into nitrides, sulfides, oxides and exogenous inclusions. The scale of standards found in the PN-64/H-04510 standard was used for this study.

2.1. AlN solubility

The solubility AlN in austenite and ferrite have been described in literature and are expressed by:

Austenite:

$$\log\left[(\%\mathrm{Al})(\%\mathrm{N})\right] = -\frac{7400}{T} + 1.95$$

Ferrite:

$$\log\left[(\%\mathrm{Al})(\%\mathrm{N})\right] = -\frac{8296}{T} + 1.69 \qquad [22]$$

Based on H. Adrian's thermodynamic model applied into a computer application Carb_Nit designed also by H. Adrian solubility curves were determined for examinate steel [23].

3. Results and discussion

The metallographic observations included 300 images of the surface of the polished specimens; example images are shown in Fig. 1. Non-metallic inclusions occurring in investigated steels were categorized into three types: sulfide type: highly malleable, single grey particles with a wide range of aspect ratios (length/width), alumina type (nitrides): numerous non-deformable, angular, black or silver-blue particles, spherical – oxide type: circular or almost circular, individual particles [24]. The identification and assignment of a given inclusion to the appropriate group of inclusions was based on their morphology shown in the TEM analysis [25].

3.1. Results of SEM-EDS analysis

In order to facilitate the identification of inclusions, EDS analyses were performed. Finding individual inclusions in both sections was problematic due to their low contribution and dispersion. Examples of the EDS results for individual inclusion are shown in Figs. 2 to 7. The individual inclusions can be distinguished by size, shape and color. Oxides are spherical in shape and black in color (Fig. 2). Sulfides are more elongated and greyish in color (Fig. 4). In contrast, the nitrides are also grey in color, but their shape is more angular (Fig. 6). The recorded EDS spectra shown in Figs. 3, 5 and 7 confirmed the contribution of the main elements included in the studied inclusions. The chemical composition of the individual inclusions is given in the TABLES 2-4 supplementing the EDS analysis. Taking into account the difficulty of the EDS method to the analysis of light elements such as O and N, the presented contents should be treated as indicative and were introduced to confirm what type of inclusion we are dealing.

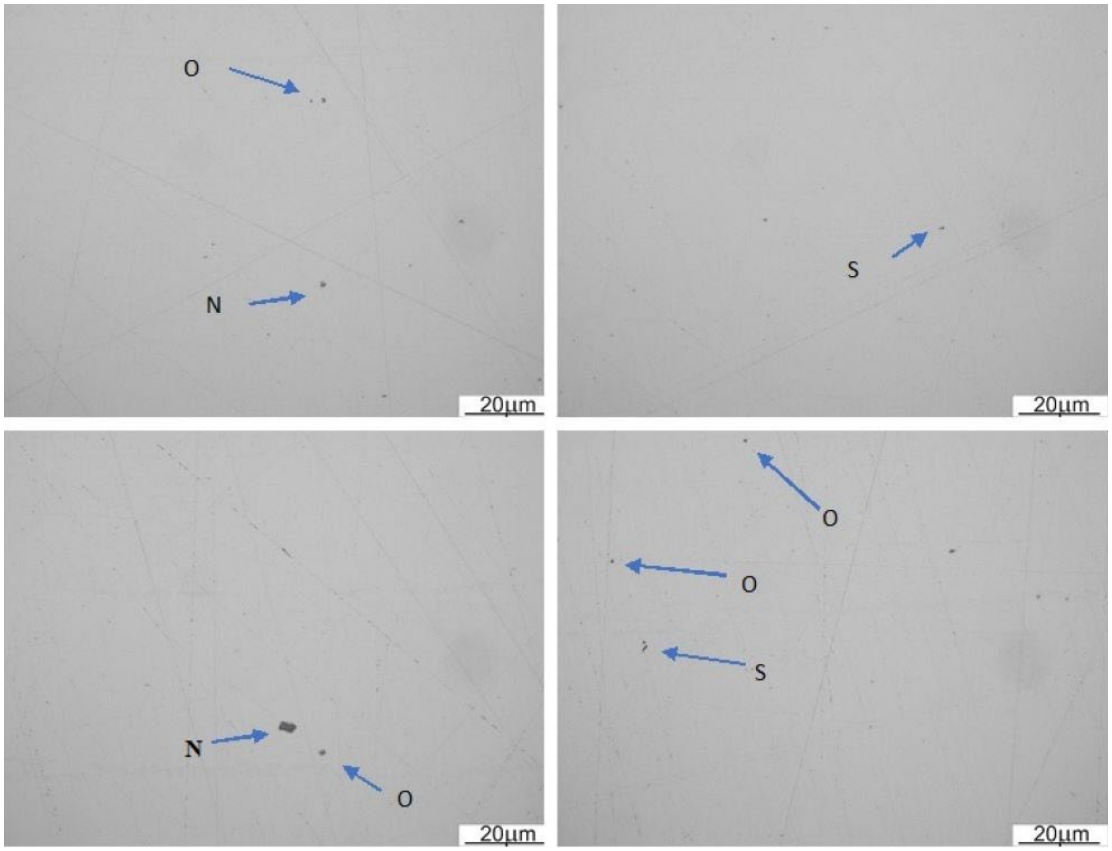

Fig. 1. Image of non-metallic inclusions on the surface of samples: N – nitrides; S – sulfides; O – oxides. LM, magnification 150×

Examples of three inclusions differing in morphology and composition are shown. The observed oxides is mainly compounds of oxygen with aluminum, as confirmed by the analysis. This is indicated by the high aluminum and oxygen content registered on the characteristic spectrum. Obtained wider EDS analysis also shows that we are faced with complex oxides too in this steel.

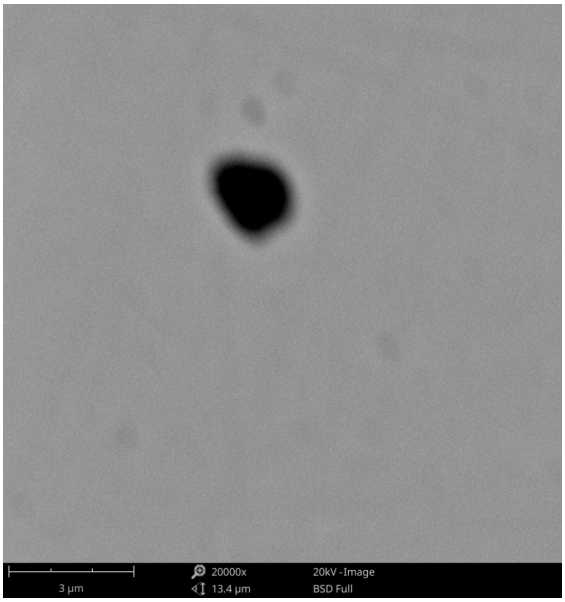

Fig. 2. Results from EDS: oxide inclusion SEM microstructure; FOV: 13.4 µm, Mode: 20 kV – Image, Detector: BSD Full

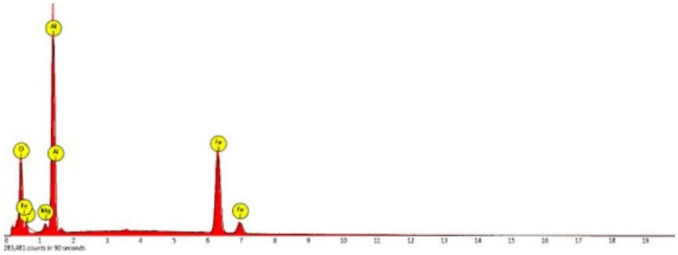

Fig. 3. Results from EDS: oxide inclusions EDS spectrum

TABLE 2

Results from EDS: chemical composition of oxide shown on Fig. 2 and spectrum Fig. 3

Element Symbol	Atomic Conc.	Weight Conc.	Stoich. wt Conc.
O*	47.57*	29.13*	
Al	34.91	36.05	50.86
Fe	15.35	32.81	46.29
Mg	2.17	2.02	2.85

* content is illustrative due to the difficulty of EDS analysis for this element

In the case of the sulfides (Fig. 4), very fine precipitates are observed. These are iron- and manganese-rich sulfides. An increased silicon content within the sulfide was also recorded which origin can be explained by high silicon content in the matrix of the steel.

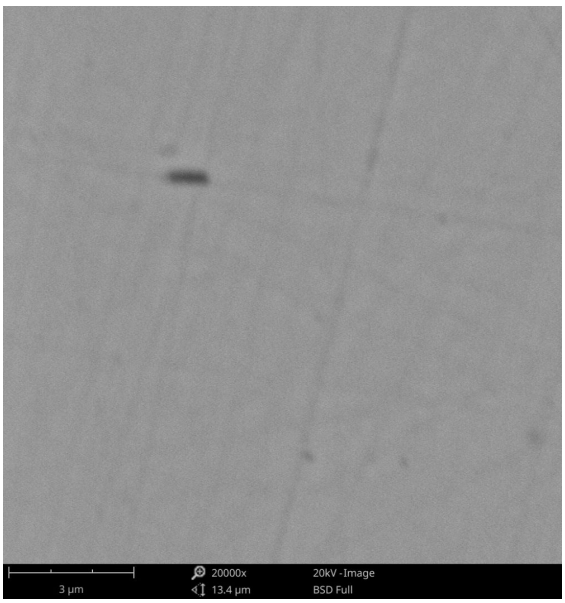

Fig. 4. Results from EDS: sulfide inclusion SEM microstructure; FOV: 13.4 µm, Mode: 20 kV – Image, Detector: BSD Full

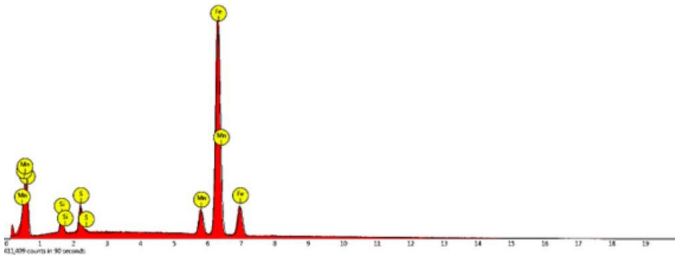

Fig. 5. Results from EDS: sulfide inclusion: EDS spectrum

TABLE 3

Results from EDS: chemical composition of sulfide shown on Fig. 4 and spectrum Fig. 5

Element Symbol	Atomic Conc.	Weight Conc.	Stoich. wt Conc.
Fe	79.86	84.79	84.79
Mn	7.69	8.03	8.03
S	7.04	4.29	4.29
Si	5.41	2.89	2.89

An inclusion, which formed a consolidated system of aluminum nitride combined with oxide and sulfide (Fig. 6) was also identified. In practice, the inclusion particles tend to be agglomerates by heterogeneous nucleation mechanism [2].

3.2. Results of metallographic observations

In most cases, single inclusions could be detected during observations, although there were also observations where there were several inclusions in one image as well as areas without inclusions.

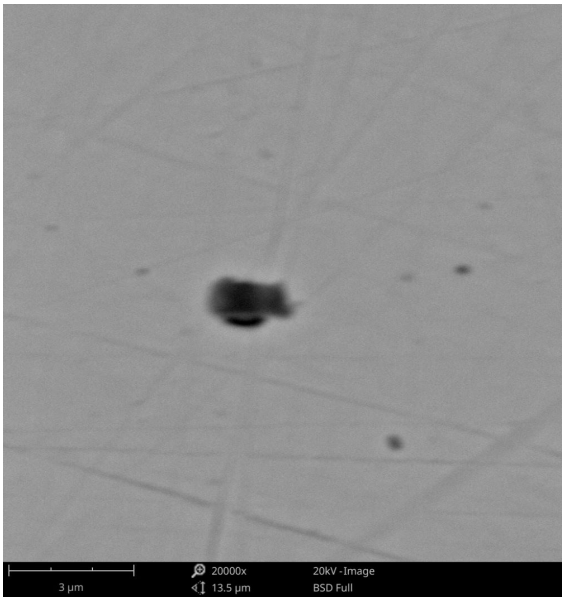

Fig. 6. Results from EDS: nitride inclusion SEM microstructure; FOV: 13.5 µm, Mode: 20 kV – Image, Detector: BSD Full

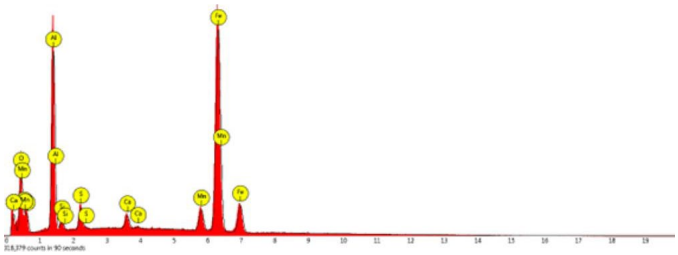

Fig. 7. Results from EDS: nitride inclusion: EDS spectrum

TABLE 4

Results from EDS: chemical composition of nitride shown on Fig. 6 and spectrum Fig. 7

Element Symbol	Atomic Conc.	Weight Conc.	Stoich. wt Conc.
N*	37.71*	18.89*	
Fe	28.14	49.21	60.67
Al	27.15	22.94	28.29
Mn	2.54	4.36	5.38
S	2.16	2.17	2.67
Si	1.25	1.10	1.35
Ca	1.06	1.33	1.64

* content is illustrative due to the difficulty of EDS analysis for this element

3.2.1. Volume fraction of nitrides in the tested samples

The highest amount of nitrides was observed in heat No. 1, while the lowest in heat No. 2. For heat No. 3, the values were very similar to heat No. 1, the difference between the two being minimal (Fig. 8). The mass ratio of Al/N is 1.9. Based on chemical composition and calculated Al/N ratio it can be noticed that heat No. 2 has the smallest ratio Al/N = 1.56 when for other 2 heats No. 1 and No. 3 it is calculated respectively 2.5 and 2.1. This ratio may explain lowest amount of nitrides in heat No. 2. It can be seen that the volume fraction of inclusions between sections varies. For the longitudinal section (Fig. 9) the smallest percentage of inclusions was obtained for heat No. 1 (less than $0.05 \cdot 10^{-3}$%), while for the other two heats the amount is at the same level (more than four times that of heat No. 1). Referring to the cross-section (Fig. 10), the opposite situation can be observed: for heat No. 1 we observe more than twice quantity of precipitates than in sample No. 3, while no inclusions of this type were observed in sample No. 2.

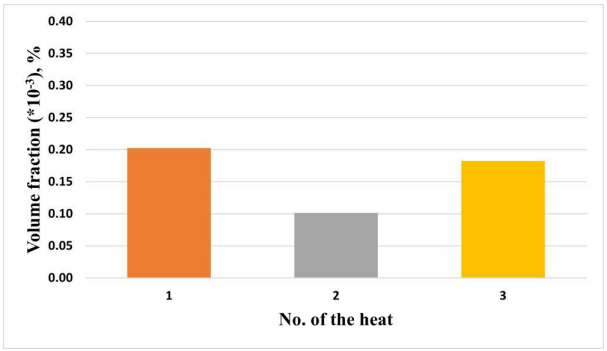

Fig. 8. Total volume fraction of nitride

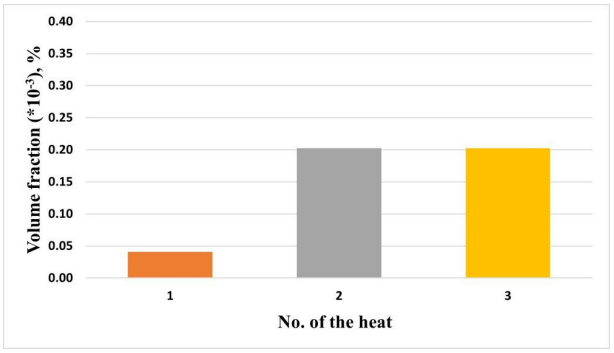

Fig. 9. Volume fraction of nitrides in specimens with longitudinal section

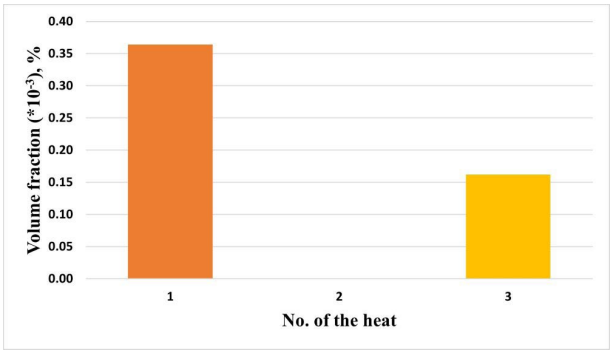

Fig. 10. Volume fraction of nitrides in specimens in cross-section

3.2.2. Volume fraction of sulfides in the tested samples

The largest volume fraction of sulfides is contained in heat No. 2, and the smallest in heat No. 3 (four times the low value than No. 2.) (Fig. 11). The Vv of inclusions in heat No. 1 is twice

as small as in sample No. 2. The Vv of sulfides in samples with a longitudinal section (Fig. 12) had a similar evolution to the total Vv of sulfides. Sulfides were easier observed in longitudinal direction which can be explained by their ability to extend along the rolling direction in deformation process. For the cross section (Fig. 13), the Vv of sulfides in heats No. 1 and 2 is twice as small as that observed in the longitudinal section, and no sulfides were observed in sample from heat No. 3.

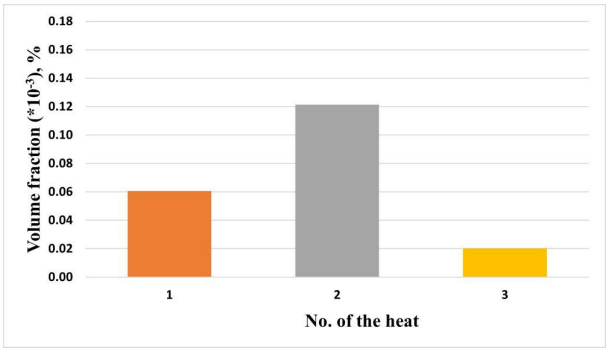

Fig. 11. Total volume fraction of sulfides

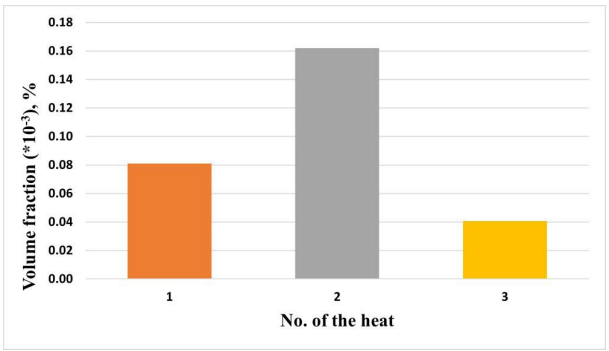

Fig. 12. Volume fraction of sulfides in specimens with longitudinal section

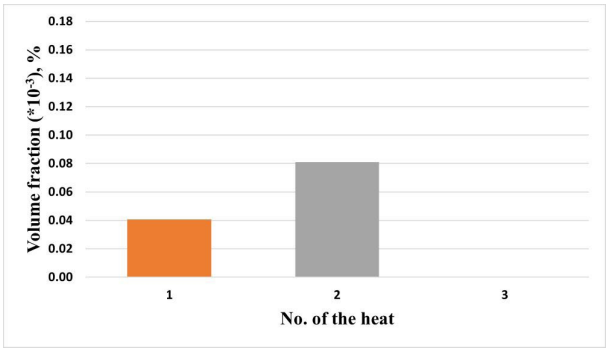

Fig. 13. Volume fraction of sulfides in specimens in cross section

3.2.3. Volume fraction of oxides in the tested samples

The largest percentage of inclusions is represented by heat No. 1, while the smallest is observed in heat No. 3. The oxide content of heat No. 3 is almost twice as low as that of heat No. 1. (Fig. 14). Fig. 15. presents the results for samples with a longitudinal section, which are similar to the summary of the total share of oxides (Fig. 14). However, for the cross section (Fig. 16). it can be noticed that the quantity of inclusions in heats No. 1 and No. 2 is at the same level.

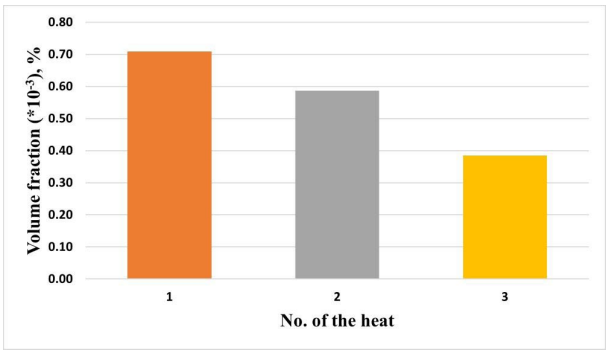

Fig. 14. Total volume fraction of oxides

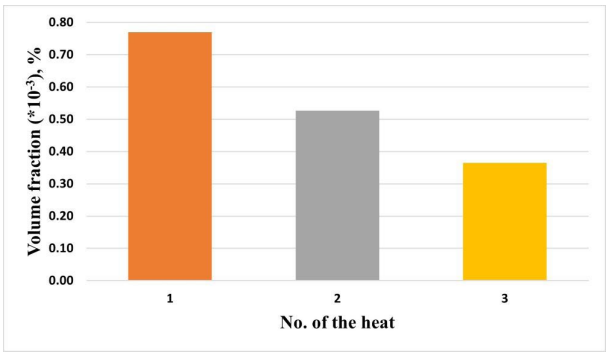

Fig. 15. Volume fraction of oxides in specimens with longitudinal section

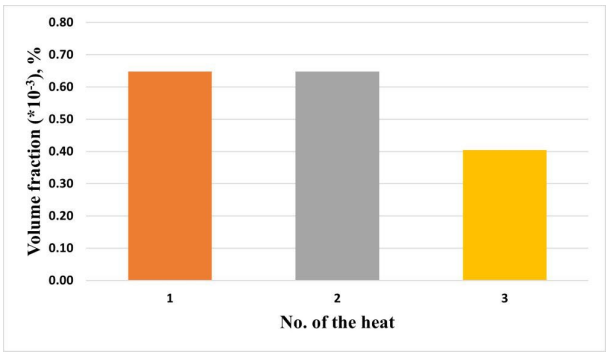

Fig. 16. Volume fraction of oxides in specimens cross-section

3.2.4. The total volume fraction of inclusions

Summarizing analysis of inclusions for all heats (Fig. 17) it can be concluded that heat No. 3 had the highest purity in terms of inclusions, which was quite well visible during the stereological analysis of examinate sample. Often, when the grid was being projected, none of the grid nodes encountered an inclusion. On the other hand, heat No. 1 is characterized by the largest number of inclusions. There is no very large disproportion between the volume fraction of inclusions analyzed on individual sections (Fig. 18.).

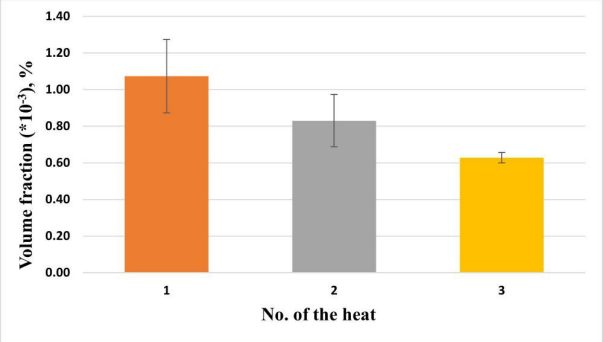

Fig. 17. Total volume fraction of all non-metallic inclusions in individual heats

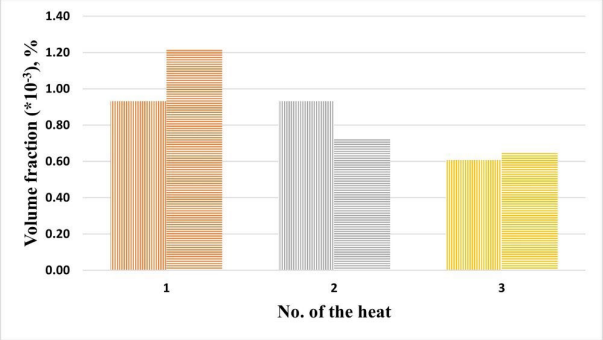

Fig. 18. Total volume fraction of all non-metallic inclusions for the given section (vertical pattern represents the longitudinal section, horizontal pattern represents the transverse section)

Aluminum exists in steel in the form of oxide inclusions, aluminum nitrides or as aluminum in solid solution. Using the Adrian's model, the theoretical ALN solubility curve were determined for the ferrite matrix of examinate steels. (Fig. 19). The temperature range at which the rolling process is carried out is plotted in gray. Based on the analysis of the solubility curve,

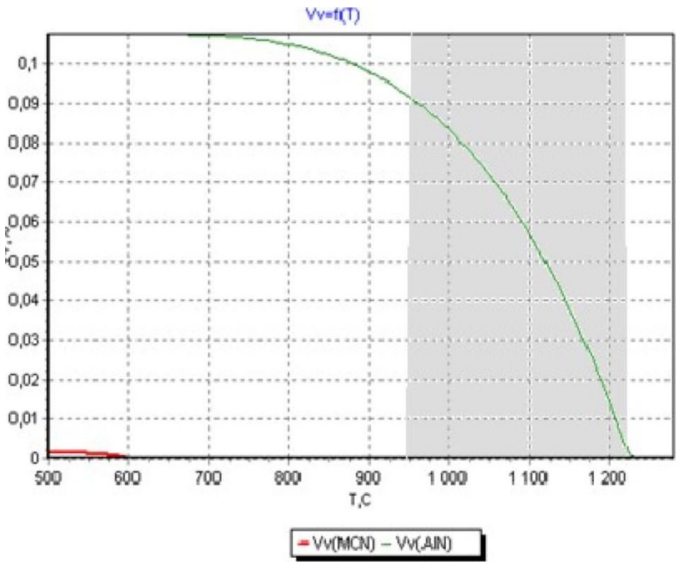

Fig. 19. Theoretical solubility curve of aluminum nitride in a ferrite matrix determined for the test steel based on the chemical composition heat No. 1

it can be concluded that in the hot-rolling range all aluminum nitride should be dissolved in order to be re-solved in the dispersed form during the cooling process.

On the aluminum nitride formation, Al + N = AlN, the stoichiometry relation between nitrogen (N) and aluminum (Al) contents on the precipitate formation is given by:

$$\mathrm{Al} = \frac{26.98}{14.01}\mathrm{N} \qquad [14]$$

Comparing the amount of oxides in each sample in relation to the oxygen content and also the Al/N ratio, it can be observed that the heat with the highest Al/N ratio also had the highest amount of oxide inclusions, while the heat with the Al/N ratio most similar to the stoichiometrically had the lowest amount of oxides (Fig. 20).

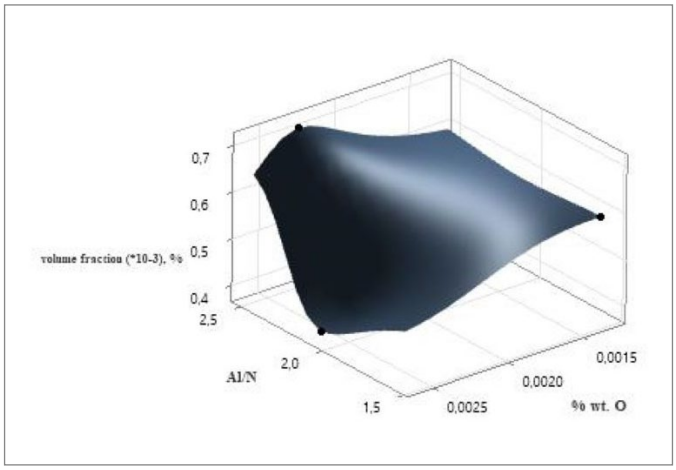

Fig. 20. Average amount of oxides in relation to the percentage of oxygen and Al/N ratio

Relating the amount of nitrides that were observed in examinate heats to the chemical composition, it can be pointed that heat No. 2 which had the lowest amount of aluminum and the lowest Al/N value also had the lowest amount of nitrides, heats 1 and 3 for which Al/N > 2 had comparable amounts of nitrides (Fig. 2).

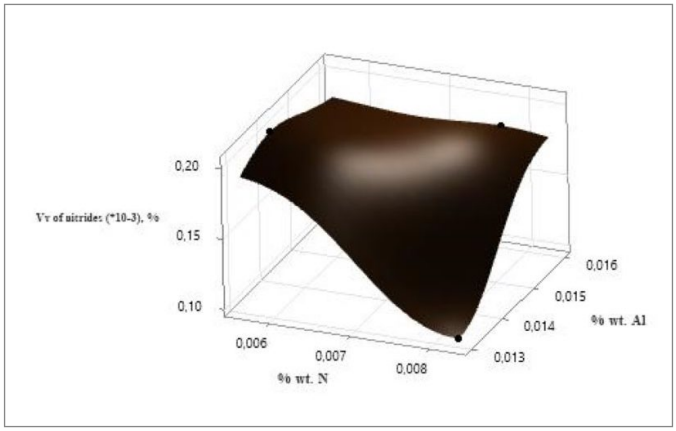

Fig. 21. Average amount of nitrides in relation to wt.% of Al and wt.% N

4. Conclusions

The research carried out in this study allowed to determine the share of non-metallic inclusions in three heats. The analyzed results presented that oxides and nitrides were the most common inclusions in the samples. Sulfides occurred sporadically. The key elements during steelmaking are the appropriate share of non-metallic inclusions so that they properly affect the properties of the steel. The appropriate share of nitrides, sulfides and oxides is achieved through a properly selected chemical composition. The three different castings analyzed were characterized by different contents of non-metallic inclusions. As well as slight differences in chemical composition. The presented results allow us to conclude that the cleanest casting was represented by heat No. 3, which was characterized by the smallest amount of non-metallic inclusions at 0.0006%. Based on the study, the following can be concluded:

- The most common type of non-metallic inclusions in the three studied casts are oxide inclusions. They represent nearly 70% of all inclusions.
- Nitrides are the second most common, which represent nearly 20% of all inclusions.
- Sulfides are observed more often and easier in the longitudinal section, which is related to their elongation in the rolling direction. Their elongated shape caused their total share in the cross-section to be smaller
- The release of aluminum nitrides is involved in hot rolling process where their dispersion occurs
- The amount of oxides and nitrides in steel can be related to the ratio of aluminum to nitrogen. If the Al/N ratio is similar to the mass theoretical ratio of these elements the amount of oxides in the steel is the smallest.

Acknowledgments

The Ministry of the Education and Science financed this work within the 5th edition of the Implementation PhD programme. The authors of this study would like to thank Ms. Katarzyna Lech for help in this research.

REFERENCES

[1] X. Zhang, S. Pirker, M. Saeedipour, Investigation of Inclusion Removal at Steel-Slag Interface toward a Small-Scale Criterion for Particle Separation. Steel Research **94** (2200842), (2023). DOI: https://doi.org/10.1002/srin.202200842

[2] T. Alatarvas, R. Podor, E.P. Heikkinen, Q. Shu, H. Singh, Revealing the Kinetics of Non-metallic Inclusion Reactions in Steel using In-situ High Temperature Environmental Scanning Electron Microscopy. Materials & Design (2023). DOI: https://doi.org/10.1016/j.matdes.2023.112139

[3] X. Zhu, W. Wan, L. Qian, Y. Cai, X. Chen, P. Zhang, G. Huang, B. Liu, Q. Yao, S. Li, Z. Yao, Research on Intelligent Identification and Grading of Nonmetallic Inclusions in Steels Based on Deep Learning. Micromachines **14** (2), 482 (2023). DOI: https://doi.org/10.3390/mi14020482

[4] S. Luo, K. Li, W. Wang, M. Zhu, Numerical simulation of macrosegregation in continuously cast slab with application of S-EMS and MR. Journal of Materials Research and Technology **24**, 6893-6907 (2023). DOI: https://doi.org/10.1016/j.jmrt.2023.04.258

[5] S. Piva, A. Nogueira Assis, P. Ch. Pistorius, M. Kan, Calcium-Treated Steel Cleanliness Prediction Using High-Dimensional Steelmaking Process Data. Integrating Materials and Manufacturing Innovation **12**, 171-184 (2023). DOI: https://doi.org/10.1007/s40192-023-00300-y

[6] D. Liu, Z. Xue, S. Song, Effect of cooling rate on non-metallic inclusion formation and precipitation and micro-segregation of Mn and Al in Fe-23Mn-10Al-0.7C steel. Journal of Materials Reaserch and Technology **24**, 4967-4979 (2023). DOI: https://doi.org/10.1016/j.jmrt.2023.04.024

[7] B. Pawłowski, J. Krawczyk, The effect of non-metallic inclusions on mechanical properties of a toughned hypoeutectoid low-alloy steel. Archives of Metallurgy and Materials **55** (1), (2010).

[8] J. Krawczyk, B. Pawłowski, The effect of non-metallic inclusions on the crack propagation impact energu of toughned 35B2+Cr steel. Metallurgy and Foundry Engineering **34** (2), (2008).

[9] G. Li, L. Wang, H. Wu, Ch. Liu, X. Wang, Z. Cui, Dissolution kinetics of the sulfide-oxide complex inclusion and resulting localized corrosion mechanism of X70 steel in deaerated acidic environment. Corrosion Scince **174** (108815), (2020). DOI: https://doi.org/10.1016/j.corsci.2020.108815

[10] E. Sidorova, A. Karasev, D. Kuznetsov, P.G. Jonsson, Investigation of the Initial Corrosion Destruction of a Metal Matrix around Different Non-Metallic Inclusions on Surfaces of Pipeline Steels. Materials **15**, 2530 (2022). DOI: https://doi.org/10.3390/ma15072530

[11] K. Jenkins, M. Lindenmo, Precipitates in electrical steels. Journal of Magnetism and Magnetic Materials **320**, 2423-2429 (2008). DOI: https://doi.org/10.1016/j.jmmm.2008.03.062

[12] M. Fernandes, J.C. Pires, N. Cheung, A.Garcia, Influence of refining time on nonmetallic inclusions in a low-carbon, silicon-killed steel. Materials Characterization **51**, 301-308 (2003). DOI: https://doi.org/10.1016/j.matchar.2004.01.003

[13] Y. Liu, C. Zhu, L. Huang, X. Chen, G. Li, Influence of Inclusions on Magnetic Properties of Al-Killed Non-oriented Silicon Steels. Magnetic Materials for Multifunctional Application (2022). DOI: https://doi.org/10.1007/s11837-022-05333-w

[14] F.L. Alcântara, R. Barbosa, M.A. Cunha, Study of Aluminum Nitride Precipitation in Fe-3%Si Steel. Materials Research **16** (5), 1039-1044 (2013). DOI: https://doi.org/10.1590/S1516-14392013005000090

[15] X. Zang, Ch. Liu, J. Qiu, Y. Wang, Effect of Al content on the agglomeration behavior of inclusions in high Al steel. Journal of Materials Reaserch and Technology **25**, 2251-2260 (2023). DOI: https://doi.org/10.1016/j.jmrt.2023.06.087

[16] S. Biorosca, A. Nadoum, D. Hawezy, F. Robinson, W. Kockelmann, Mechanistic approach of Goss abnormal grain growth in electrical

steel: Theory and argument. Acta Materialia **185**, 370-381 (2020). DOI: https://doi.org/10.1016/j.actamat.2019.12.023

[17] C. Yilmaz, M. Poul, L. Lahn, D. Raabe, S. Zaefferer, Dislocation-assisted Particle Dissolution: A New Hypothesis for Abnormal Growth of Goss Grains in Grain-oriented Electrical Steels. Acta Materialia, (2023). DOI: https://doi.org/10.1016/j.actamat.2023.119170

[18] Q. Gao, J. Li, X. Wang, J. Gong, B.Li, Characteristic of Precipitate Evolution during High Temperature Annealing in Grain-Oriented Silicon Steel. Metals **12**, 824, (2022). DOI: https://doi.org/10.3390/met12050824

[19] H. Liu, S. Yao, Y. Sun, F. Gao, H. Song, G. Liu, D. Geng, z. Liu, G.Wang, Evolution of microstructure, texture and inhibitor along the processingroute for grain-oriented electrical steels using strip casting. Materials Characterization **106**, 273-282 (2015). DOI: http://dx.doi.org/10.1016/j.matchar.2015.06.010

[20] C. Zhu, Y. Liu, Y. Xiao, W. Yan, G. Li, A New Review on Inclusion and Precipitate Control in Grain-Oriented Silicon Steels. The Minerals, Metals & Materials Society (2022). DOI: https://doi.org/10.1007/s11837-022-05345-6

[21] A. Wac-Włodarczyk, Materiały magnetyczne. Modelowanie i zastosowania, Politechnika Lebelska, Lublin (2012).

[22] F.G Wilson, T. Gladman, Aluminium nitride in steel. International Materials Reviews **5** (33), 221-286 (1988). DOI: https://doi.org/10.1179/imr.1988.33.1.221

[23] H. Adrian, Thermodynamic model for precipitation of carbonitrides in high strength low alloy steels containing up to three microalloying elements with or without additions of aluminium. Materials Science and Technology **8**, 406-420 (1992). DOI: https://doi.org/10.1179/mst.1992.8.5.406

[24] X. Zhu, W. Wan, L. Qian, Y. Cai, X. Chen, P. Zhang, G. Huang, B. Liu, Q. Yao, S. Li, Z. Yao, Research on Intelligent Identification and Grading of Nonmetallic Inclusions in Steels Based on Deep Learning. Micromachines (2023). DOI: https://doi.org/10.3390/mi14020482

[25] V. Vodárek, A. Volodarskaja, S. Miklušová, J. Holešinský, O. Žáček, Precipitation Reactions in a Copper – Bearing GOES. Procedia Materials Science **12**, 77-82 (2016). DOI: https://doi.org/10.1016/j.mspro.2016.03.014